Physics in the edge of fusion devices

Felix I. Parra, Michael Barnes and Michael Hardman
Rudolf Peierls Centre for Theoretical Physics, University of Oxford, Oxford OX1 3PU, UK

(This version is of 23 April 2021)

1. Introduction

We present a brief overview of the current state of fusion device edge modeling. This report is written for ExCALIBUR NEPTUNE contract T/NA085/20. This contract stated mission is the development of kinetic models for the edge. Thus, this report will focus on the known problems of fluid models without making much emphasis on their many successes. This lack of praise for fluid models is not the objective of this report and hence we would like to start by reassuring the reader that we believe current fluid codes have much to offer and need to be pursued in parallel to kinetic modeling. One of the challenges for kinetic modeling is to devise methods to match with fluid simulations efficiently. With this capability, the edge can be split into non-overlapping spatial regions with different levels of kinetic sophistication.

The remainder of this reports is organized as follows. In section 2 we explain what the characteristic time and length scales are in the edge. In section 3, we give an overview of the existing fluid models for the edge. In section 4 we list physical phenomena that cannot be captured by fluid models, and we explain how these phenomena have been addressed so far. Finally, we discuss our proposal to develop a complete set of kinetic equations for the edge in section 5.

2. The edge

In this report, we call the edge the plasma that surrounds the separatrix. The separatrix (represented as a red line in figure 1) is the flux surface that separates the region where magnetic field lines are in contact with the walls of the vessel from the region in which magnetic field lines form nested toroidal flux surfaces. This means that the edge includes both **open field lines** (those who are in contact with walls) and **closed field lines** (those that form nested toroidal flux surfaces).

We need to distinguish the core, where the fusion reactions are supposed to take place, from the edge. In this report, we will use a theoretical criterion to distinguish one from the other: whether the characteristic transit times in the directions parallel and perpendicular to the magnetic field are comparable or not. In the core, both ions and electron closely follow magnetic field lines and can travel around the device many times before collisions, turbulent fluctuations or other effects drive them away from the magnetic field line on which they started. As a result, density and temperature are almost constant along magnetic field lines, and one only worries about small fluctuations around the mostly quiescent profiles of density and temperature. This is, of course, a highly idealized situation that ignores violent events taking place in the core, such as sawteeth (Hastie 1997), but it is a useful one.

In contrast, in the edge, charged particles that were well-confined in the core region cross the separatrix and eventually reach the wall by following magnetic field lines. The displacements of ions and electrons away from the magnetic field line in which they

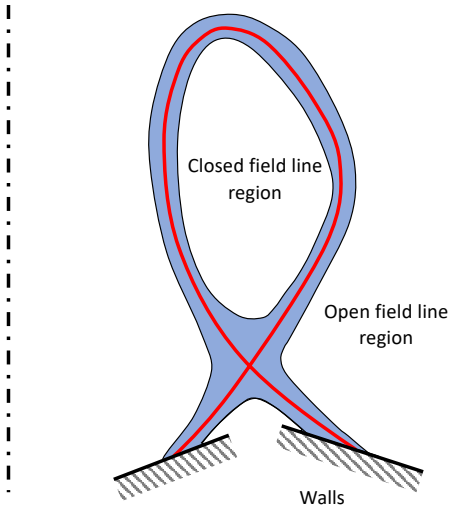

FIGURE 1. Sketch of a tokamak edge on a plane that contains the axis of symmetry (represented here by a dash-dot vertical line). The edge region is in blue, and the separatrix is the red line.

started are still small compared to the size of the device, but they are not small compared with the characteristic lengths of the density and temperature in the edge region. If the characteristic lengths of density and temperature along and across magnetic field lines are $L_\parallel$ and $L_\perp$, the edge is characterized by

$$\frac{|v_\parallel|}{L_\parallel} \sim \frac{|\mathbf{v}_d|}{L_\perp}, \tag{2.1}$$

where $v_\parallel$ is the characteristic parallel velocity of the particles, and $\mathbf{v}_d$ their small drift perpendicular to the magnetic field. Since $|v_\parallel| \gg |\mathbf{v}_d|$, $L_\perp$ is much smaller than $L_\parallel$. In the core, for comparison, we find that $L_\parallel$ and $L_\perp$ are of similar order and comparable to the machine size, giving

$$\frac{|v_\parallel|}{L_\parallel} \gg \frac{|\mathbf{v}_d|}{L_\perp}. \tag{2.2}$$

There is another aspect that makes the edge very different from the core. The temperature of both electrons and ions is kept low near the wall because the wall is a very effective sink of energy (wall materials that prevent slow Hydrogen particles from going back into the plasma are notable exceptions where the temperature of the plasma can be large near the wall; see, for example, Schmitt *et al.* (2015) for liquid Lithium divertors, or Jackson *et al.* (1991) for boronized walls). At low plasma temperatures, the plasma is partially ionized and collisions between the charged particles in the plasma and neutrals become important. In extreme limits, detachment occurs, that is, the plasma temperature decreases sufficiently due to radiation that the plasma recombines and a cushion of neutrals appears in front of the walls protecting them (Krasheninnikov & Kukushkin 2017).

In addition to limiting the temperature, the presence of the wall controls the size of the electric field and the flows in the open field line region. We will discuss these effects in more detail in section 3.

We finish this section by calculating a few characteristic time and length scales. In Militello & Fundamenski (2011), one can find a concise summary of typical values of plasma characteristics in the edge of tokamaks. In current tokamaks, the magnitude of

the magnetic field B is typically 2 T, and the characteristic size of the device is a few meters. The plasma temperature T ranges from 1 keV in the closed magnetic field line part of the edge to 100 eV at the separatrix down to 10 eV near the wall. In detached plasmas, the temperature drops to 1 eV near the wall. The electron density n_e ranges from 10^{19} m^{-3} in the open field line region to 10^{20} m^{-3} in the closed field line region. Neutral density n_n is usually smaller than n_e and it ranges from 10^{15} m^{-3} in the closed field line region to 10^{19} m^{-3} in the open field line region (Colchin *et al.* 2000; Scotti *et al.* 2021). With these quantities, we calculate several characteristic frequencies of interest:

• The gyrofrequencies of both Deuterium and electrons, $\Omega_i := eB/m_D$ and $\Omega_e := eB/m_e$, are the characteristic frequencies of the nearly circular motion of the charged particles around magnetic field lines. Here e is the proton charge, and m_D and m_e are the Deuterium and electron masses.

• The transit frequencies for Deuterium ions and electrons, $v_{tD}/L_\parallel$ and $v_{te}/L_\parallel$, are the inverse of the time that it takes charged particles to move along a magnetic field line from one wall to another in the open field line region, and the inverse of the time that it takes charged particles to sample a flux surface in the closed field line region. Here $v_{tD} := \sqrt{2T/m_D}$ and $v_{te} := \sqrt{2T/m_e}$ are the Deuterium and electron thermal speeds, and $L_\parallel$ is the characteristic length of magnetic field lines in the edge, which we take to be 10 m.

• The transit frequency for Deuterium neutrals, $v_{tD}/L_\perp$, is the inverse of the time that it takes neutral atoms to cross the edge region. The characteristic scale of variation of density and temperature across magnetic field lines, $L_\perp$, is of the order of 5 cm or larger in the closed field line region (Sugihara *et al.* 2000), and of the order of 1 cm or larger in the open field line region (Goldston 2012).

• The collision frequencies

$$\nu_{ii} := \frac{4\sqrt{\pi}}{3}\frac{e^4 n_e \ln\Lambda}{(4\pi\epsilon_0)^2 m_D^{1/2} T^{3/2}} \tag{2.3}$$

and

$$\nu_{ep} := \frac{4\sqrt{2\pi}}{3}\frac{e^4 n_e \ln\Lambda}{(4\pi\epsilon_0)^2 m_e^{1/2} T^{3/2}} \tag{2.4}$$

describe how often Deuterium ions collide with each other or electrons collide with other electrons or Deuterium ions, respectively. Here $\ln\Lambda \approx 15$ is the Coulomb logarithm and ϵ_0 is the vacuum permittivity. The factor of $\sqrt{2}$ difference between ν_{ii} and ν_{ep} is a convention introduced by Braginskii (Braginskii 1958).

• We also need the collision frequencies that describe how often Deuterium ions collide with Deuterium neutral atoms, $\nu_{in} := n_n v_{tD}\sigma_{in}$, and how often Deuterium neutral atoms collide with Deuterium ions, $\nu_{ni} := n_i v_{tD}\sigma_{in}$. Here, the ion-neutral cross section σ_{in} is of order 10^{-18} m^2 (Lindsay & Stebbings 2005). Similarly, we need the collision frequencies that describes how often electrons collide with Deuterium neutral atoms, $\nu_{en} := n_n v_{te}\sigma_{en}$, and how often neutrals are ionized, $\nu_{\rm ion} := n_e v_{te}\sigma_{\rm ion}$. Here, the electron-neutral collision cross section σ_{en} is of order 10^{-19} m^2 (Brackmann *et al.* 1958) and the ionization collision cross section $\sigma_{\rm ion}$ is of order 10^{-20} m^2 (Zel'dovich & Raizer 2013).

All these frequencies are shown in table 1. It is clear that the collision frequencies are the ones that change the most across the edge. For ions and electrons, collisions become very important in the cooler plasma of the open field line region, but are infrequent in the closed field line region. Conversely, for neutrals, collision are more frequent in the closed field line region than in the open field line region.

We also calculate a few length scales of interest:

	Ion freq. [10^4 s^{-1}]				Neutral freq. [10^4 s^{-1}]			Electron freq. [10^6 s^{-1}]			
Region	Ω_i	$v_{tD}/L_\parallel$	ν_{ii}	ν_{in}	$v_{tD}/L_\perp$	ν_{ni}	$\nu_{\rm ion}$	Ω_e	$v_{te}/L_\parallel$	ν_{ep}	ν_{en}
Closed lines	9400	3.1	0.16	0.031	610	3100	1800	320000	1.8	0.13	0.0018
Open lines	9400	0.31	16	31	310	31	18	320000	0.18	13	1.8

TABLE 1. Characteristic frequencies for the closed field line region ($B = 2$ T, $n_e = 10^{20}$ m^{-3}, $n_n = 10^{15}$ m^{-3}, $T = 1$ keV) and the open field line region ($B = 2$ T, $n_e = 10^{19}$ m^{-3}, $n_n = 10^{19}$ m^{-3}, $T = 10$ eV).

	Parallel lengths [1 m]					Perpendicular lengths [1 cm]				
Region	$L_\parallel$	λ_{ii}	λ_{in}	λ_{ep}	λ_{en}	$L_\perp$	ρ_i	ρ_e	λ_{ni}	$\lambda_{\rm ion}$
Closed lines	10	190	1000	140	10000	5	0.33	0.0056	1	1.7
Open lines	10	0.19	0.1	0.14	1	1	0.033	0.00056	10	17

TABLE 2. Characteristic lengths for the closed field line region ($B = 2$ T, $n_e = 10^{20}$ m^{-3}, $n_n = 10^{15}$ m^{-3}, $T = 1$ keV) and the open field line region ($B = 2$ T, $n_e = 10^{19}$ m^{-3}, $n_n = 10^{19}$ m^{-3}, $T = 10$ eV).

- The mean free paths $\lambda_{ii} := v_{tD}/\nu_{ii}$ and $\lambda_{in} := v_{tD}/\nu_{in}$ are the distances that a Deuterium ion can travel before colliding with another Deuterium ion or with a Deuterium atom, respectively. Similarly, the mean free paths $\lambda_{ni} := v_{tD}/\nu_{ni}$ and $\lambda_{\rm ion} := v_{tD}/\nu_{\rm ion}$ are the distances that a Deuterium neutral atom can move before colliding with an ion or getting ionized, respectively, and $\lambda_{ep} := v_{te}/\nu_{ep}$ and $\lambda_{en} := v_{te}/\nu_{en}$ are the distances that an electron can move before colliding with another charged particle or with a neutral, respectively.
- The Deuterium and electron gyroradii, $\rho_i := v_{tD}/\Omega_i$ and $\rho_e := v_{te}/\Omega_e$, are the characteristic size of the gyration of charged particles around magnetic field lines.

All these lengths are given in table 2. Unsurprisingly, we see that the mean free paths, inversely proportional to the collision frequencies, are the characteristic lengths that change the most across the edge. In the direction perpendicular to the magnetic field, we see that the gyroradii are small compared to the characteristic lengths.

3. Drift-ordered fluid models

Due to the large collision frequencies in the open field line region, the bulk of the ion and electron distribution functions is Maxwellian. For this reason, much of the edge modeling has been based on plasma fluid equations derived in the limit of large Coulomb collisions (Braginskii 1958). Since the most readily available fluid equations for magnetized plasmas assume that there are no neutrals, most fluid models ignore neutrals, with some notable exceptions.

The main difference between the fluid equations used in edge models and the usual fluid equations is that diffusivities are anisotropic. As demonstrated by table 1, charged particles gyrate around magnetic field lines many times before having a collision. Thus, particles barely move across magnetic field lines and the diffusivity across magnetic field lines is much smaller than the diffusivity along them. To capture the effect of this anisotropy correctly and efficiently, one has to either use flux coordinates that follow magnetic field lines (Beer *et al.* 1995) or employ appropriate discretizations (Hariri & Ottaviani 2013).

The problem with following magnetic field lines is that it is difficult to find a grid that both aligns with the magnetic field lines and extends to the walls of the vessel. Unfortunately, the wall geometry is important because it determines how far neutrals leaving the wall travel into the plasma (Wiesen *et al.* 2018). Finding grids that adjust to the wall geometry has become a problem of great interest in recent years, and the community has been trying exotic methods to address it (Isoardi *et al.* 2010; Bufferand *et al.* 2019).

An important aspect of the edge fluid models is the size of the flow. The potential difference between the wall and the plasma is controlled by the non-neutral Debye sheath that forms around the walls (Riemann 1991). Typically, the potential drop between the wall and the plasma has to be several times the electron temperature because otherwise a large electron current flows into the wall, breaking the neutrality of the plasma. If one assumes that the wall in contact with the plasma is a conductor and hence the potential is constant across its volume, the potential differences within the plasma are restricted to be of the order of the electron temperature, $\phi \sim T/e$. This gives an electric field $\mathbf{E} = -\nabla\phi$ of the order of $T/eL_\perp$. The perpendicular velocity of the fluid is determined by the balance between the electric and magnetic forces,

$$\mathbf{u}_\perp \times \mathbf{B} \sim \mathbf{E}. \tag{3.1}$$

This equation gives a perpendicular velocity of order

$$\mathbf{u}_\perp \sim \frac{|\mathbf{E}|}{B} \sim \frac{\rho_i}{L_\perp} v_{tD}. \tag{3.2}$$

Thus, according to table 2, $\mathbf{u}_\perp$ is significantly smaller than v_{tD}.

The fluid equations obtained with the ordering (3.2) are known as **drift-ordered** equations because the flow is of the same order as the slow particle drifts – the other possible ordering is the **high flow** ordering that assumes that the perpendicular velocity is sonic. Importantly, for fluid velocities of the size given in equation (3.2), one needs to keep terms that depend on the gradient of the temperature and the pressure in the stress tensor to be completely consistent (Mikhailovskii & Tsypin 1971; Simakov & Catto 2003; Catto & Simakov 2004).

The system of drift-ordered fluid equations is usually comprised of

- one continuity equation per ion species (the electron density need not be calculated because it is determined by quasineutrality),
- one conservation equation for the component of the plasma momentum parallel to the magnetic field,
- a vorticity equation that determines the electrostatic potential,
- in electromagnetic models, Ampére's law, and
- one conservation equation for the energy of all ion species and another one for the energy of the electrons.

Note that there is one single conservation equation for the whole plasma parallel momentum and one single conservation equation for the energy of all the ion species, and not several conservation equations, one per ion species. The reason why all ion species must be considered as one in these fluid equations is that, within the large collision frequency approximation, all ion species have the same temperature and all charged species have the same average flow. The electron temperature can be different from the ion temperature due to the mass difference between the two species. The temperature differences between the different ion species are of the same order as kinetic effects that are neglected. The differences between the parallel flows are calculated and used in the vorticity equation, where they are needed because the electric current enters in the Lorenz force.

As we mentioned at the start, the drift-ordered fluid equations usually implemented

in edge codes (Mikhailovskii & Tsypin 1971; Simakov & Catto 2003; Catto & Simakov 2004) ignore neutrals. There have been attempts to include neutrals in the limit where both ions and neutrals are sufficiently collisional that both species can be treated as fluids (Hazeltine *et al.* 1992; Catto 1994; Helander *et al.* 1994). The advantage of these models is that they account for the effect that ion-neutral collisions have on the diffusivities, but it is generally believed that these models are insufficient because neutrals have long mean free paths in large regions of the edge (see tables 1 and 2). There have been some attempts at simplified kinetic treatments of the neutrals (Wersal & Ricci 2015) and there exist sophisticated Monte-Carlo approaches with a large collection of collisions such as EIRENE (Reiter *et al.* 2005) or DEGAS (Stotler & Karney 1994). Note that these Monte-Carlo treatments are not completely self-consistent because they assume that the ion and electron distribution functions are Maxwellian and, depending on the version of the code, they ignore elastic collisions and they average over the dependence of the differential cross section on the scattering angle. Moreover, these neutral kinetic codes are sensitive to the parameters that determine how particles interact with the wall (Chankin *et al.* 2021), and these parameters are not well known.

There are two types of problems in which the drift-ordered fluid equations are used: 2D profiles and turbulence. The objective of 2D fluid solvers such as SOLPS (Wiesen *et al.* 2015), SolEdge2D (Bufferand *et al.* 2015), UEDGE (Rognlien *et al.* 2007) or EDGE2D (Simonini *et al.* 1994) is to determine the toroidally averaged density and temperature profiles in the edge. These codes cannot model turbulent fluctuation because they are missing the third dimension. For this reason, instead of the collisional perpendicular diffusion coefficients, these codes use enhanced perpendicular diffusion coefficients that are chosen to match the experimental observations. These 2D codes are meant to provide detailed understanding of transport along magnetic field lines and of neutrals, as some of them are coupled to Monte-Carlo neutral codes such as EIRENE (Reiter *et al.* 2005) or DEGAS (Stotler & Karney 1994).

Turbulence codes such as GBS (Halpern *et al.* 2016), TOKAM3X (Tamain *et al.* 2016), Hermes (Dudson & Leddy 2017) or GRILLIX (Stegmeir *et al.* 2018) are 3D fluid codes. Originally, fluid turbulence codes assumed that ions were much colder than electrons and that the turbulent fluctuations were small compared to an almost constant background (Zeiler *et al.* 1996). However, it was soon realized that this treatment is not appropriate for the edge. Ions are not cold and the density and temperature profiles cannot be easily split into a slowly varying piece plus small fluctuations due to the presence of the wall. The same wall boundary conditions that constrain the fluid velocity perpendicular to the magnetic field to be subsonic, as shown in equation (3.2), require that the fluid velocity parallel to the magnetic field be sonic near the wall (Chodura 1982). The pressure drops along magnetic field lines have to be significant to ensure that the parallel flow is accelerated sufficiently. This is incompatible with the assumption that the fluctuations are small. Thus, most current edge turbulence codes have tried to lift the assumption of small fluctuations, and they have done so by differing degrees depending on the code or the version of the code in use.

Overall, fluid codes are maturing, and although there is still work to be done, there is starting to be a consensus on the physics that they must include. The same cannot be said about kinetic effects in the edge.

4. Kinetic effects

Tables 1 and 2 are evidence that kinetic effects must be taken into account: in the closed magnetic field line region and in part of the open field line region, ions and electrons can

travel a distance of the size of the device without suffering a single collision. Moreover, kinetic effects are surprisingly important even in the regions where the collision frequency is high. There are two reasons for this.

- The diffusive heat flux calculated in the fluid limit is only accurate if $\nu_{ep} \gtrsim 100\, v_{te}/L_{\|}$ because the heat flux is dominated by energetic particles that collide much less than the thermal particles (Gurevich & Istomin 1979; Gray & Kilkenny 1980). The fluid solution assumes that there are too many energetic particles in the hot plasma regions, and predicts too few energetic particles in the cooler regions. This is a well known issue, and in 2D fluid simulations, it is resolved by imposing an upper bound for the electron heat flux that is of order $n_e T v_{te}$.
- The other region where kinetic effects are important is near the wall. The ions and electrons that reach the wall recombine and do not come back as charged particles. As a result of this recombination, the charged particle distribution functions vanish for significant parts of the velocity space and cannot be approximated by Maxwellians, as one would need to be the case to be able to use fluid equations. Thus, the treatment of charged particles near the wall has to be kinetic (Loizu *et al.* 2011; Geraldini *et al.* 2018). The combination of these two issues can manifest in a population of energetic electrons that cannot be predicted by fluid models. In turn, these energetic electrons affect the density and temperature by suppressing or enhancing heat transport and by changing the potential difference across the Debye sheaths. Evidence of these effects has been found in direct kinetic simulations of 1D problems (Tskhakaya *et al.* 2011; Chankin & Coster 2015).

The fact that kinetic effects are important has been recognized for neutrals, leading to kinetic codes for them (Reiter *et al.* 2005; Stotler & Karney 1994). However, as we have pointed out before, these codes ignore any possible non-Maxwellian features in the ion and electron distribution functions, are sensitive to the parameters that determine how particles interact with the wall and, depending on the version, do not include many elastic collisions or detailed collision physics. The non-Maxwellian features of the electron distribution function are particularly important as electrons mediate many of the processes considered important in these neutral models: radiation, ionization, recombination, etc.

For ions and electrons, the community is starting to construct edge kinetic codes such as XGC (Ku *et al.* 2016), GKEYLL (Hakim *et al.* 2020) or COGENT (Dorf *et al.* 2016). These codes are broadly based on the same gyroaveraged kinetic models used in δf gyrokinetic codes such as GS2 (Kotschenreuther *et al.* 1995; Dorland *et al.* 2000), GENE (Dannert & Jenko 2005) or stella (Barnes *et al.* 2019), but are very different from them because of the edge particularities, as we proceed to explain. The idea behind gyroaveraged kinetic models is to average over the fast gyrofrequency time scale to avoid a cripplingly small time step. All gyroaveraged kinetic models are based on an asymptotic expansion in $\rho_i/L_{\perp} \ll 1$ (see table 2 for values of ρ_i and $L_{\perp}$). The simplest possible approach is drift kinetics (Hazeltine 1973) that assumes that the size of all turbulent structures is much larger than ρ_i. Unfortunately, in the presence of temperature and density gradients, drift kinetics develops instabilities at the grid scale. These instabilities can be stabilized by numerical dissipation, and in the real word, they are stabilized by finite gyroradius effects that drift kinetics neglects. Gyrokinetics (Catto 1978; Frieman & Chen 1982) was developed to solve this problem in the core of the tokamak. Initially, δf gyrokinetics assumed that turbulent fluctuations had a characteristic size of the order of ρ_i and their amplitude was small by a factor of $\rho_i/L_{\perp} \ll 1$. This ensures that the gradients of the fluctuations are comparable to the background gradient and not larger.

However, as we have explained in section 3, in the edge it is not possible to assume that density and temperature are slowly varying quantities plus small fluctuations. This fact

was part of the justification to develop what is know as full f gyrokinetics, in which the distribution function is not assumed to be composed of a slowly varying piece plus small fluctuations. See Parra & Catto (2008) and Brizard & Hahm (2007) for two different types of derivations of full f gyrokinetics. Overall, full f gyrokinetics can be seen as a mixture of drift kinetics and the original δf gyrokinetics. The distribution function is allowed to have wavelengths that range from $L_\perp$ to ρ_i, but the size of these different Fourier components has to be sufficiently small that the gradient of the distribution function is never larger than $1/L_\perp$. Assuming a core ordering (2.2), one naturally recovers δf gyrokinetics, showing that the distribution function has to be a slowly varying piece plus small fluctuations (Parra & Catto 2010; Calvo & Parra 2012).

In the edge ordering (2.1), full f gyrokinetics fundamentally becomes drift kinetics with some small corrections. These corrections are of two types.

- The electromagnetic fields appear in the kinetic equation averaged over circular gyro-orbits. Thus, electromagnetic fluctuations that have characteristic lengths much smaller than the gyroradius are averaged over and do not drive fluctuations in the distribution function. Since these short wavelength electromagnetic fluctuations can only survive if there are charge and current fluctuations of similar wavelength, which they are not able to drive, they eventually damp and disappear.
- The field equations, quasineutrality and Ampére's law, contain densities and currents that one calculates from the ion and electron distribution functions. As a result of the gyrokinetic expansion, these distribution functions have finite gyroradius corrections that give terms that are small in $\rho_i/L_\perp \ll 1$. One of these small terms in particular, the polarization density in the quasineutrality equation, is important because, despite its small size, it can determine the electric field in different situations. For example, for shear Alfven waves, the polarization density is small, but so are the rest of the contributions to the density, so in the end a balance between the polarization density and another term determines the fluctuating electric field. Another example is the component of the electric field perpendicular to the flux surfaces, which is also determined by a balance between the polarization density and other terms (Parra & Catto 2009).

The small finite gyroradius terms in the full f gyrokinetic equations are important to stabilize the short wavelength instabilities, and some of them (e.g. the polarization density) can also be important for certain aspects of the physics. Keeping the finite gyroradius effects in the kinetic equation is relatively straightforward in PIC codes, although one has to be careful with the accuracy of the average (Guadagni & Cerfon 2017). We are not aware of any full f edge gyrokinetic code that retains finite gyroradius effects in the kinetic equation.

The corrections to the field equations are much more difficult to retain – formulations that explicitly try to conserve energy and momentum exactly require solving nonlinear equations for every element in velocity space, for instance. This has driven the community towards simplifying these terms. As a result of these simplifications, several edge codes solve drift kinetics with some *ad hoc* additions to the field equations, such as a simplified polarization density.

In addition to these fundamental issues, edge drift kinetics and gyrokinetics need to address other problems. As gyrokinetics was devised to model turbulent fluctuations with a spatial size of the order of ρ_i in tokamak cores, most available models do not include features that are important for edge physics.

- There is no gyrokinetic formulation for the wall boundary conditions. Only recently one such formulation was developed for drift kinetic ions in magnetic fields that reach the wall with a grazing angle (Geraldini *et al.* 2018). This work has to be generalized to

electrons, more general angles between the wall and the magnetic field, and eventually to gyrokinetics.

• Gyrokinetics does not usually include collisions with neutrals, and such collisions are important because neutrals break the symmetry introduced by the fast charged particle gyration around magnetic field lines. In other words, the dependence on gyrophase, neglected in gyrokinetics, can become important.

• Gyrokinetics was developed for fluctuations with characteristic scales of the order of the ion gyroradius. At these scales, the magnetic field fluctuations have a very constrained form. For this reason, the extension of gyrokinetics to include MagnetoHydroDynamic (MHD) modes is non-trivial and an active area of research. See Zheng *et al.* (2007) for a theoretical treatment, and Collar *et al.* (2020) for recent numerical work in this area. A gyrokinetic model of the edge should be able to reproduce MHD results, as MHD modes are believed to be the main drive of the eruptions known as Edge Localized Modes (ELMs) (Ham *et al.* 2020).

5. Discussion

A complete edge description requires kinetic effects. Current attempts to model kinetic effects in the edge rely heavily on gyroaveraged kinetic models that average over the very fast gyrofrequency timescale.

In our opinion, there does not exist a systematic procedure to choose the relevant finite gyroradius effects to be kept in the kinetic and field equations. The first objective of a kinetic modeling effort for the edge must be to establish the finite gyroradius effects to be kept in the equations. To do so, for contract T/NA085/20, we have proposed as a first attempt to construct a drift kinetic model. This drift kinetic model will be unstable at grid scales, but hyperviscosity might be enough to stabilize such scales if they do not contribute much to transport (as one would expect due to their small size). For the contract work, we will use the model only in 1D and 2D configurations that cannot develop these grid scale instabilities. We will then determine analytically which finite gyroradius effects must be kept in the equations to determine every part of the problem, and in particular the component of the electric field perpendicular to the flux surfaces.

A well known issue arises when keeping finite gyroradius effects in the field equations. In quasineutrality, the only term that contains the electric potential explicitly is the small finite gyroradius correction. Thus, unless an implicit time stepping algorithm is employed, one needs to solve for the potential by inverting a small term in the equation. This procedure limits the time step size severely (Lee 1987; Barnes *et al.* 2019). Thus, in addition to keeping finite gyroradius effects, we need to make sure that the kinetic equations that we obtain are amenable to implicit time stepping methods.

In addition to studying finite gyroradius effects, we will determine the effect that collisions with neutrals have on the gyrokinetic formalism by introducing charge exchange collisions and ionization collisions.

The final deliverable of contract T/NA085/20 will be a drift kinetic model with neutrals and the finite gyroradius terms that are needed to calculate the component of the electric field that is perpendicular to the flux surfaces. Both of these features will be improvements on the models implemented in existing continuum edge codes.

By the end of the contract, the model will have been tested in 1D and 2D problems, and even though it will have a 3D version, this 3D version will not have been tested in the turbulent regime. Moreover, all the work will have been performed in a helical field and not in a diverted tokamak field because the helical field is the state-of-the-art for continuum edge kinetic codes (only recently, in the 2020 Annual APS DPP meeting, the

two leading continuum codes, GKEYLL and COGENT, have reported the first runs with more complex tokamak geometry). The limitations of the model delivered at the end of contract T/NA085/20 leave two obvious avenues for future work.

• The main theoretical difficulty added by tokamak magnetic fields is the presence of a component of the drifts in the direction perpendicular to the flux surface that does not exist in the case of a helical field. This component of the drifts leads to finite orbit widths and can significantly modify some of the physics of both quiescent 2D plasmas (Kagan & Catto 2008; Landreman *et al.* 2014) and 3D turbulence (Parisi *et al.* 2020). Adding this component of the particle drift to the equations will require extra work.

• As we have explained above, the 3D model is expected to have grid scale instabilities that can be stabilized by hyperviscosity or other numerical methods of dissipation. To properly capture the fluctuations at the ion gyroradius scale, one would have to include more precise finite gyroradius effects. This is an obvious extension of the work in contract T/NA085/20, and it is very important for High confinement mode (H-mode) where the turbulence at scales larger than the ion gyroradius is stabilized for still unclear reasons. In this regime, turbulence at scales of the order of or smaller than the ion gyroradius is important (Hillesheim *et al.* 2016; Hatch *et al.* 2017; Parisi *et al.* 2020), and the finite gyroradius effects become crucial for ions. We foresee that adding more detailed finite gyroradius effects will be theoretically and numerically challenging and will require dedicated work.

Two other aspects of an edge kinetic model are beyond the scope of contract T/NA085/20.

• To test the effect of wall boundary conditions on drift kinetics, we will impose a simplified version of the boundary conditions that are valid in the limit in which the electron gyroradius is much smaller than the Debye length. However, more detailed boundary conditions must be found because usually the electron gyroradius is larger than or comparable to the Debye length. This is work that is being pursued by one of the authors of this report (F.I.P.) with other sources of funding.

• We pointed out above that it would be desirable to be able to recover MHD modes with the edge kinetic model. In the work for contract T/NA085/20, the fluctuations in the magnetic field will be neglected (this is a good approximation for many edge plasmas), and hence it will not be possible to explore connections with MHD. This is an area of research where ExCALIBUR NEPTUNE could benefit from collaboration with the EPSRC Programme Grant 'Turbulent Dynamics of Tokamak Plasmas (TDoTP)'. Several PIs in the ExCALIBUR NEPTUNE project also belong to TDoTP.

REFERENCES

Barnes, M., Parra, F.I. & Landreman, M. 2019 stella: An operator-split, implicit-explicit δf-gyrokinetic code for general magnetic field configurations. *J. Comput. Phys.* **391**, 365.

Beer, M.A., Cowley, S.C. & Hammett, G.W. 1995 Field-aligned coordinates for nonlinear simulations of tokamak turbulence. *Phys. Plasmas* **2**, 2687.

Brackmann, R.T., Fite, W.L. & Neynaber, R.H. 1958 Collisions of Electrons with Hydrogen Atoms. III. Elastic Scattering. *Phys. Rev.* **112**, 1157.

Braginskii, S.I. 1958 Transport phenomena in a completely ionized two-temperature plasma. *Sov. Phys. JETP* **6**, 358.

Brizard, A.J. & Hahm, T.S. 2007 Foundations of nonlinear gyrokinetic theory. *Rev. Mod. Phys.* **79**, 421.

Bufferand, H., Ciraolo, G., Marandet, Y., Bucalossi, J., Ghendrih, Ph., Gunn, J., Mellet, N., Tamain, P., Leybros, R., Fedorczak, N., Schwander, F. & Serre, E. 2015 Numerical modelling for divertor design of the WEST device with a focus on plasmawall interactions. *Nucl. Fusion* **55**, 053025.

Bufferand, H., Tamain, P., Baschetti, S., Bucalossi, J., Ciraolo, G., Fedorczak, N.,

Ghendrih, Ph., Nespoli, F., Schwander, F. & E. Serre and, Y. Marandet 2019 Three-dimensional modelling of edge multi-component plasma taking into account realistic wall geometry. *Nucl. Mat. Energy* **18**, 82.

Calvo, I. & Parra, F.I. 2012 Long-wavelength limit of gyrokinetics in a turbulent tokamak and its intrinsic ambipolarity. *Plasma Phys. Control. Fusion* **54**, 115007.

Catto, P.J. 1978 Linearized gyro-kinetics. *Plasma Phys.* **20**, 719.

Catto, P.J. 1994 A short mean-free path, coupled neutral-ion transport description of a tokamak edge plasma. *Phys. Plasmas* **1**, 1936.

Catto, P.J. & Simakov, A.N. 2004 A drift ordered short mean free path description for magnetized plasma allowing strong spatial anisotropy. *Phys. Plasmas* **11**, 90.

Chankin, A.V., Corrigan, G. & JET Contributors 2021 EDGE2D-EIRENE modeling of the impact of wall materials on core edge, scrape-off layer and divertor parameters. *Plasma Phys. Control. Fusion* **63**, 035010.

Chankin, A.V. & Coster, D.P. 2015 On the locality of parallel transport of heat carrying electrons in the SOL. *J. Nucl. Mater.* **463**, 498.

Chodura, R. 1982 Plasma-wall transition in an oblique magnetic field. *Phys. Fluids* **25**, 1628.

Colchin, R.J., Maingi, R., Fenstermacher, M.E., Carlstrom, T.N., Isler, R.C., Owen, L.W. & Groebner, R.J. 2000 Measurement of neutral density near the X point in the DIII-D tokamak. *Nucl. Fusion* **40**, 175.

Collar, J.P.M., McMillan, B.F., Saarelma, S. & Bottino, A. 2020 Comparing electromagnetic instabilities in global gyrokinetic simulations with local and MHD models. *Plasma Phys. Control. Fusion* **62**, 095005.

Dannert, T. & Jenko, F. 2005 Gyrokinetic simulation of collisionless trapped-electron mode turbulence. *Phys. Plasmas* **12**, 072309.

Dorf, M.A., Dorr, M.R., Hittinger, J.A., Cohen, R.H. & Rognlien, T.D. 2016 Continuum kinetic modeling of the tokamak plasma edge. *Phys. Plasmas* **23**, 056102.

Dorland, W., Jenko, F., Kotschenreuther, M. & Rogers, B.N. 2000 Electron Temperature Gradient Turbulence. *Phys. Rev. Lett.* **85**, 5579.

Dudson, B.D. & Leddy, J. 2017 Hermes: global plasma edge fluid turbulence simulations. *Plasma Phys. Control. Fusion* **59**, 054010.

Frieman, E.A. & Chen, L. 1982 Nonlinear gyrokinetic equations for low-frequency electromagnetic waves in general plasma equilibria. *Phys. Fluids* **25**, 502.

Geraldini, A., Parra, F.I. & Militello, F. 2018 Solution to a collisionless shallow-angle magnetic presheath with kinetic ions. *Plasma Phys. Control. Fusion* **60**, 125002.

Goldston, R.J. 2012 Heuristic drift-based model of the power scrape-off width in low-gas-puff H-mode tokamaks. *Nucl. Fusion* **52**, 013009.

Gray, D.R. & Kilkenny, J.D. 1980 The measurement of ion acoustic turbulence and reduced thermal conductivity caused by a large temperature gradient in a laser heated plasma. *Plasma Phys.* **22**, 81.

Guadagni, J. & Cerfon, A.J. 2017 Fast and spectrally accurate evaluation of gyroaverages in non-periodic gyrokinetic Poisson simulations. *J. Plasma Phys.* **83**, 905830407.

Gurevich, A. & Istomin, Ya.N. 1979 Thermal runaway and convective heat transport by fast electrons in a plasma. *Sov. Phys. JETP* **50**, 470.

Hakim, A.H., Mandell, N.R., T.N. Bernard and, M. Francisquez, Hammett, G.W. & Shi, E. L. 2020 Continuum electromagnetic gyrokinetic simulations of turbulence in the tokamak scrape-off layer and laboratory devices. *Phys. Plasmas* **27**, 042304.

Halpern, F.D., Ricci, P., Jolliet, S., Loizu, J., Morales, J., Mosetto, A., Musil, F., Riva, F., Tran, T.M. & Wersal, C. 2016 The GBS code for tokamak scrape-off layer simulations. *J. Comput. Phys.* **315**, 388.

Ham, C., Kirk, A., Pamela, S. & Wilson, H. 2020 Filamentary plasma eruptions and their control on the route to fusion energy. *Nature Rev. Phys.* **2**, 159.

Hariri, F. & Ottaviani, M. 2013 A flux-coordinate independent field-aligned approach to plasma turbulence simulations. *Comput. Phys. Comm.* **184**, 2419.

Hastie, R.J. 1997 Sawtooth instability in tokamak plasmas. *Astrophys. Space Sci.* **256**, 177.

Hatch, D.R., Kotschenreuther, M., Mahajan, S., Valanju, P. & Liu, X. 2017 A gyrokinetic perspective on the JET-ILW pedestal. *Nucl. Fusion* **57**, 036020.

Hazeltine, R.D. 1973 Recursive derivation of drift-kinetic equation. *Plasma Phys.* **15**, 77–80.

Hazeltine, R.D., Calvin, M.D., Valanju, P.M. & Solano, E.R. 1992 Analytical calculation of neutral transport and its effect on ions. *Nucl. Fusion* **32**, 3.

Helander, P., Krasheninnikov, S.I. & Catto, P.J. 1994 Fluid equations for a partially ionized plasma. *Phys. Plasmas* **1**, 3174.

Hillesheim, J.C., Dickinson, D., Roach, C.M., Saarelma, S., Scannell, R., Kirk, A., Crocker, N.A., Peebles, W.A., Meyer, H. & the MAST Team 2016 Intermediate-k density and magnetic field fluctuations during inter-ELM pedestal evolution in MAST. *Plasma Phys. Control. Fusion* **58**, 014020.

Isoardi, L., Chiavassa, G., Ciraolo, G., Haldenwang, P., Serre, E., Ghendrih, Ph., Sarazin, Y., Schwander, F. & Tamain, P. 2010 Penalization modeling of a limiter in the Tokamak edge plasma. *J. Comput. Phys.* **229**, 2220.

Jackson, G.L., Winter, J., Taylor, T.S., Burrell, K.H., DeBoo, J.C., Greenfield, C.M., Groebner, R.J., Hodapp, T., Holtrop, K., Lazarus, E.A., Lao, L.L., Lippmann, S.I., Osborne, T.H., Petrie, T.W., Phillips, J., James, R., Schissel, D.P., Strait, E.J., Turnbull, A.D., West, W.P. & the DIII-D Team 1991 Regime of very high confinement in the boronized DIII-D tokamak. *Phys. Rev. Lett.* **67**, 3098.

Kagan, G. & Catto, P.J. 2008 Arbitrary poloidal gyroradius effects in tokamak pedestals and transport barriers. *Plasma Phys. Control. Fusion* **50**, 085010.

Kotschenreuther, M., Rewoldt, G. & Tang, W.M. 1995 Comparison of initial value and eigenvalue codes for kinetic toroidal plasma instabilities. *Comput. Phys. Comm.* **88**, 128.

Krasheninnikov, S.I. & Kukushkin, A.S. 2017 Physics of ultimate detachment of a tokamak divertor plasma. *J. Plasma Phys.* **83**, 155830501.

Ku, S., Hager, R., Chang, C.S., Kwon, J.M. & Parker, S.E. 2016 A new hybrid-Lagrangian numerical scheme for gyrokinetic simulation of tokamak edge plasma. *J. Comput. Phys.* **315**, 467.

Landreman, M., Parra, F.I., Catto, P.J., Ernst, D.R. & Pusztai, I. 2014 Radially global δf computation of neoclassical phenomena in a tokamak pedestal. *Plasma Phys. Control. Fusion* **56**, 045005.

Lee, W.W. 1987 Gyrokinetic particle simulation model. *J. Comput. Phys.* **72**, 243.

Lindsay, B.G. & Stebbings, R.F. 2005 Charge transfer cross sections for energetic neutral atom data analysis. *J. Geophys. Res.* **110**, A12213.

Loizu, J., Ricci, P. & Theiler, C. 2011 Existence of subsonic plasma sheaths. *Phys. Rev. E* **83**, 016406.

Mikhailovskii, A.B. & Tsypin, V.S. 1971 Transport equations and gradient instabilities in a high pressure collisional plasma. *Plasma Phys.* **13**, 785.

Militello, F. & Fundamenski, W. 2011 Multi-machine comparison of drift fluid dimensionless parameters. *Plasma Phys. Control. Fusion* **53**, 095002.

Parisi, J.F., Parra, F.I., Roach, C.M., Giroud, C., Dorland, W., Hatch, D.R., Barnes, M., Hillesheim, J.C., Aiba, N. & Ball, J. 2020 Toroidal and slab ETG instability dominance in the linear spectrum of JET-ILW pedestals. *Nucl. Fusion* **60**, 126045.

Parra, F.I. & Catto, P.J. 2008 Limitations of gyrokinetics on transport time scales. *Plasma Phys. Control. Fusion* **50**, 065014.

Parra, F.I. & Catto, P.J. 2009 Vorticity and intrinsic ambipolarity in turbulent tokamaks. *Plasma Phys. Control. Fusion* **51**, 095008.

Parra, F.I. & Catto, P.J. 2010 Turbulent transport of toroidal angular momentum in low flow gyrokinetics. *Plasma Phys. Control. Fusion* **52**, 045004.

Reiter, D., Baelmans, M. & Börner, P. 2005 The EIRENE and B2-EIRENE Codes. *Fusion Sci. Tech.* **47**, 172.

Riemann, K.-U. 1991 The Bohm criterion and sheath formation. *J. Phys. D: Appl. Phys.* **24**, 493.

Rognlien, T.D., Rensink, M.E. & Smith, G.R. 2007 User manual for the UEDGE edge-plasma transport code. *Tech. Rep.* UCRL-ID-137121. Lawrence Livermore National Laboratory.

Schmitt, J.C., Bell, R.E., Boyle, D.P., Esposti, B., Kaita, R., Kozub, T., LeBlanc, B.P., Lucia, M., Maingi, R., Majeski, R., Merino, E., Punjabi-Vinoth, S., Tchilingurian, G., Capece, A., Koel, B., Roszell, J., Biewer, T. M., Gray, T. K., Kubota,

S., Beiersdorfer, P., Widmann, K. & Tritz, K. 2015 High performance discharges in the Lithium Tokamak eXperiment with liquid Lithium walls. *Phys. Plasmas* **22**, 056112.

Scotti, F., Stotler, D.P., Bell, R.E., LeBlanc, B.P., Sabbagh, S.A., Soukhanovskii, V.A., Umansky, M.V. & Zweben, S.J. 2021 Outer midplane neutral density measurements and H-mode fueling studies in NSTX-U. *Nucl. Fusion* **61**, 036002.

Simakov, A.N. & Catto, P.J. 2003 Drift-ordered fluid equations for field-aligned modes in low-β collisional plasma with equilibrium pressure pedestals. *Phys. Plasmas* **10**, 4744.

Simonini, R., Corrigan, G., Radford, G., Spence, J. & Taroni, A. 1994 Models and Numerics in the Multi-Fluid 2-D Edge Plasma Code EDGE2D/U. *Contrib. Plasma Phys.* **34**, 368.

Stegmeir, A., Coster, D., Ross, A., Maj, O., Lackner, K. & Poli, E. 2018 GRILLIX: a 3D turbulence code based on the flux-coordinate independent approach. *Plasma Phys. Control. Fusion* **60**, 035005.

Stotler, D. & Karney, C. 1994 Neutral Gas Transport Modeling with DEGAS 2. *Contrib. Plasma Phys.* **34**, 392.

Sugihara, M., Igitkhanov, Yu., Janeschitz, G., Hubbard, A.E., Kamada, Y., Lingertat, J., Osborne, T.H. & Suttrop, W. 2000 A model for H mode pedestal width scaling using the International Pedestal Database. *Nucl. Fusion* **40**, 1743.

Tamain, P., Bufferand, H., Ciraolo, G., Colin, C., Galassi, D., Ph.Ghendrih, Schwander, F. & Serre, E. 2016 The TOKAM3X code for edge turbulence fluid simulations of tokamak plasmas in versatile magnetic geometries. *J. Comput. Phys.* **321**, 606.

Tskhakaya, D., Jachmich, S., Eich, T., Fundamenski, W. & JET EFDA contributors 2011 Interpretation of divertor Langmuir probe measurements during the ELMs at JET. *J. Nucl. Mater.* **415**, S860.

Wersal, C. & Ricci, P. 2015 A first-principles self-consistent model of plasma turbulence and kinetic neutral dynamics in the tokamak scrape-off layer. *Nucl. Fusion* **55**, 123014.

Wiesen, S., Brezinsek, S., Bonnin, X., Delabie, E., Frassinetti, L., Groth, M., Guillemaut, C., Harrison, J., Harting, D., Henderson, S., Huber, A., Kruezi, U., Pitts, R.A., Wischmeier, M. & JET contributors 2018 On the role of finite grid extent in SOLPS-ITER edge plasma simulations for JET H-mode discharges with metallic wall. *Nucl. Mat. Energy* **17**, 174.

Wiesen, S., Reiter, D., Kotov, V., Baelmans, M., Dekeyser, W., Kukushkin, A.S., Lisgo, S.W., Pitts, R.A., Rozhansky, V., Saibene, G., Veselova, I. & Voskoboynikov, S. 2015 The new SOLPS-ITER code package. *J. Nucl. Mater.* **463**, 480.

Zeiler, A., Biskamp, D., Drake, J.F. & Guzdar, P.N. 1996 Three-dimensional fluid simulations of tokamak edge turbulence. *Phys. Plasmas* **3**, 2951.

Zel'dovich, Ya. B. & Raizer, Yu. P. 2013 *Physics of Shock Waves and High-Temperature Hydrodynamic Phenomena*. Dover Publications.

Zheng, L.J., Kotschenreuther, M.T. & Dam, J.W. Van 2007 Revisiting linear gyrokinetics to recover ideal magnetohydrodynamics and missing finite Larmor radius effects. *Phys. Plasmas* **14**, 072505.